Evaluating the Performance of Geosynthetic Reinforced Soil-Integrated Bridge System (GRS-IBS) under Working Stress Condition

Murad Abu-Farsakh[1,*], *Allam* Ardah[1], and *George* Voyiadjis[2]

[1]Louisiana Transportation Research Center, Louisiana State University, Baton Rouge, LA 70808
[2]Department of Civil and Environmental Engineering, Louisiana State University, Baton Rouge, LA 70803

Abstract. This paper evaluates the performance of geosynthetic reinforced soil-Integrated Bridge System (GRS-IBS) in terms of lateral facing deformation and strain distribution along geosynthetics. Simulations were conducted using 2D PLAXIS program. The hardening model proposed by Schanz et al. [1] was used to simulate the behavior of backfill material; the backfill-reinforcement interface was simulated using Mohr-Coulomb model, and the reinforcement and facing block were simulated using linear elastic models. The numerical model was verified using the results of a case study conducted at Maree Michel GRS-IBS, Louisiana. Parametric study was carried out to investigate the effects of span length, reinforcement spacing, and reinforcement stiffness on the performance of GRS-IBS. The results indicate that span length have significant impact on strain distribution along geosynthetics and lateral facing deformation. The reinforcement stiffness has significant impact on the GRS-IBS behavior up to a certain point, beyond which the effect tends to decrease contradictory to reinforcement spacing that has a consistent relationship between the GRS-IBS behavior and reinforcement spacing. The results also indicate that reinforcement spacing has higher influence on the lateral facing deformation than the reinforcement stiffness for the same reinforcement strength/spacing ratio (T_f/S_v) due to the composite behavior of closely reinforcement spacing.

1 Introduction

The composite behavior of internally supported reinforced soil, the Geosynthetic Reinforced Soil walls (GRS), has advantages over the traditional concrete walls due to the ease of construction, cost saving, and construction time. In addition to the support of the self-weight of the backfill soil, the GRS walls can support the roadway structures and traffic loads [2-6]. A relatively new use of this system is in bridge application [Geosynthetic Reinforced Soil-Integrated Bridge System (GRS-IBS)], which can help reduce both the bridge construction time and cost [e.g. 7-13] The GRS-IBS usually includes a GRS abutment, bearing bed reinforced zone, GRS integrated approach, and a reinforced soil foundation [14]. The GRS-IBS can be used to integrate the bridge structure with the approaching road to create a jointless bridge system. Two versions of GRS-IBS are defined by the FHWA, one version uses steel girders with either a CIP footing or a precast sill. Another version of GRS-IBS uses adjacent concrete box beams supported directly on the GRS abutment without a concrete footing. Many numerical studies have been conducted on the behavior of a free-standing geosynthetic mechanically stabilized earth (GMSE) walls [e.g. 15-22]. A few numerical studies were conducted recently to evaluate the composite behavior of the GRS-IBS [e.g. 23-27, 12].

2 Numerical model

The two-dimensional finite element program PLAXIS 2D 2016 [28] was used in the current study to evaluate the effect of different parameters on the performance of GRS-IBS. Mesh refinement was first conducted to find the optimum mesh-size where the numerical results are not mesh-size dependent. The dimensions of the model domain were selected far enough to minimize the effect of boundary conditions on the model response. The lateral boundaries were fixed by roller support to prevent the soil movement in the horizontal direction. The bottom of soil foundation was fixed using bin support to prevent the soil from movement in both the horizontal and vertical directions.

The model was successfully developed and used to simulate the behavior of Maree Michel GRS-IBS [7-9] during the construction stages and after the bridge was opened to traffic. The Maree Michel Bridge was constructed by the Louisiana Department of Transportation and Development (LA DOTD) in Vermilion Parish in 2016. The total height of the GRS-IBS wall is 3.8 m from the top of the RSF and was divided into 20 layers to simulate the field construction process by using the staged construction mode in PLAXIS 2D 2016, which allows for simulation of construction and excavation processes. A 63 kPa distribution load at the top and bottom and exposed faces

* Corresponding author: cefars@lsu.edu

© The Authors, published by EDP Sciences. This is an open access article distributed under the terms of the Creative Commons Attribution License 4.0 (http://creativecommons.org/licenses/by/4.0/).

of each soil layer was applied during the staged construction process to simulate the soil compaction. This approach is based on the procedure introduced by Dantas [29] to consider the induced stress on the backfill soil due to compaction, which was also adopted later by Ehrlich and Mirmoradi [30], Mirmoradi and Ehrlich [20, 31]. The triaxial and large direct shear testing method were conducted to evaluate the strength and stiffness of the backfill materials properties. A total of three triaxial testing were conducted at three different confining pressures of 207, 345, and 483 kPa for a soil specimen size of 15.24 cm diameter and 30.48 cm height. Fig. 1 presents the simulated and measured stress-strain curve for the backfill materials [32]. Six large direct shear tests having with dimension size of 30.48 × 30.48 × 15.24 cm were conducted to evaluate the strength properties and the interface friction angle between the geosynthetic and the backfill/facing block materials. The block/soil interface friction is 27.7° based on a previous study conducted by Ling et al. [33]. A jointless interface between the bridge slab and the integrated approach was simulated based on FHWA [14]. The interface between the bridge and the footing was simulated with a friction coefficient of 0.4 [26]. The tests were conducted under normal stresses of 48.3, 120, and 191.7 kPa, which results in peak stresses of 83.5, 144, and 260 kPa, respectively. The dilation angle was estimated using the following reference [34];

$$\phi_p = \phi_{cr} + 0.8\psi \quad (1)$$

Where: ϕ_p = peak friction angle = 51°; ϕ_{cr} = critical state friction angle = 34°; ψ = dilation angle.

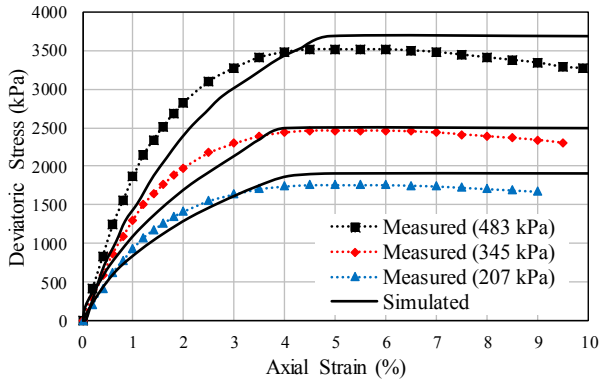

Fig. 1. Comparison of simulated and measured triaxial results.

In the current study, the configuration of the GRS-IBS numerical model is selected according to the FHWA design criteria recommendation [14]. Figure 2 presents the configuration of the GRS-IBS model that was adopted to perform the parametric study. The height of bridge abutment H was selected with a minimum span length L_{span} larger than 7.6 m, the minimum base width B_{total} *is* the greater value of 1.83 m or 0.3H. The width of the reinforced soil footing (RSF) B_{rsf} is equal to B_{total} +0.25B_{total}, assuming the bridge span to depth ratio = L_{span}/D = 24 as reported by Zheng and Fox [27], and the depth of the RSF D_{rsf} is equal to 0.25 B_{total}. The setback distance between the back of the face and the footing a_b is equal to 0.2 m. The minimum clear space d_e, the distance from the top of the facing block to the bottom of the superstructure, is equal to 8 cm or 2% of the abutment height, whichever is greater. The width of the beam seat (strip footing in this study) b was selected equal to 1.2 m with a thickness of 0.6 m (note that the minimum width of the beam seat for a span length greater than 7.6 m is 0.77 m and the minimum thickness is 0.2 m). The minimum reinforcement length L_r at the bottom of the bridge abutment should be 0.3H or B_{total}, whichever is greater, which increases linearly up to 0.7H. The bearing bed reinforcement zone was extended from the top reinforcement layer for six consecutive layers. The length of the bearing bed reinforcement L_{rb} is equal to 2a_b+b.

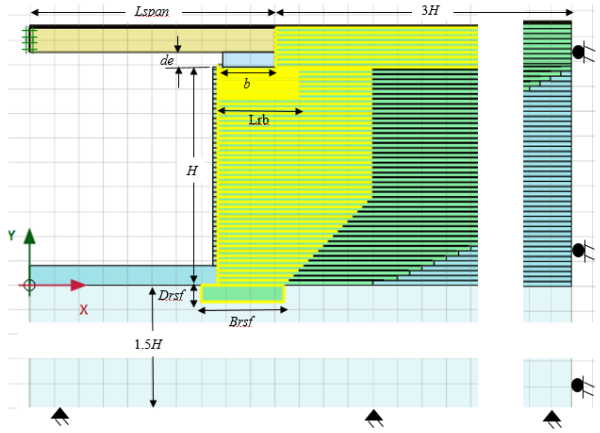

Fig. 2. GRS-IBS numerical model with geometry and boundaries conditions.

Table 1. Materials properties.

Category	Description
Facing Block	Linear elastic model; E = 3×10^7 kPa,; γ=12.5 kN/m^3; dimensions, 40.64×20.32×20.32 cm; Poisson's ratio, ν = 0
Geotextile	linear elastic perfectly plastic model; Tensile strength @ 2% = 13×17 kN/m, Tensile strength @ 5% = 35×40 kN/m; Tult = 80 kN/m; reinforcement spacing = 0.2 m; Axial stiffness, EA[1]= 600 kN/m.
Backfill Material	Hardening soil model; dry unit weight, γ_d= 18 kN/m /m^3; cohesion, c =20 kPa; friction angle, ϕ =51°; dilation angle ψ =21°; E_{50}^{ref}=34,000 kPa, E_{ur}^{ref}= 103,200 kPa, E_{oed}^{ref}=26,400, ν= 0.2; power, m = 0.5
Foundation Soil	Soil model, Mohr-Coulomb model; dry unit weight, γ_d= 15.2 kN/m^3; wet unit weight, γ_w=18.65 kN/m^3; cohesion, c=17.7 kPa; ϕ = 27°; E =30000 kPa; ν = 0.2.
Interface (backfill and geotextile)	linear elastic with Mohr-Coulomb failure criterion; adhesion, c=8.6 kPa; interface friction angle δ=40.4°
Interface (block and geotextile)	linear elastic with Mohr-Coulomb failure criterion; cohesion, c=7 kPa; friction angle ϕ = 34°
Riprap	Linear elastic model, E^b = 50 MPa; γ= 22 kN/m^3; ν = 0.25

3 Effect of span length

Five different span lengths, L_{span}, were considered and evaluated in this study: 12.2 m, 18.3 m, 24.4 m, 30.5 m, and 36.6 m, which is corresponding to applied loads on top of GRS-IBS equal to 74, 108, 145, 180, and 216 kPa, respectively. Fig. 3 presents the effect of span length on the strain distribution along the reinforcement at 20, 40, 60, and 80% of the abutment height as measured from the bottom of the abutment. It can be seen that the maximum strain envelope is located near the abutment face at 0.2 *H* and moving about 1.2 m away from the abutment face at 0.8 *H* for all cases. It can be seen that increasing the span length does not affect the shape of the strain distribution; and at the same time slightly shifting the locus of maximum strain to the left. However, increasing the span length results increasing the magnitude of strain. The maximum strain increases from 0.4% for span length of 12.2 m to around 0.9% for a span length of 36.6 m at 0.6 *H* and 0.6 *H* above the bottom of the abutment. Fig. 4 presents the effect of span length on the lateral displacement of wall facing. It can be seen that by increasing the span length, the lateral facing displacement increases, and the location of maximum displacement shifts up. The lateral facing displacement increases from 12 mm for the 12.1 m span length to 30 mm for the 36.6 m span length. The figures indicate that the span length has a significant effect on the GRS-IBS performance in terms of the strain distribution along the reinforcement and the lateral displacement of wall facing for the same abutment height (7.0 m) under service loading condition.

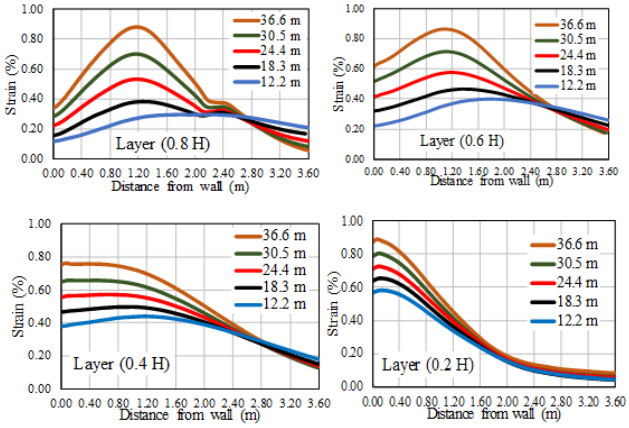

Fig. 3. Effect of span length on the strain distribution along geosynthetics.

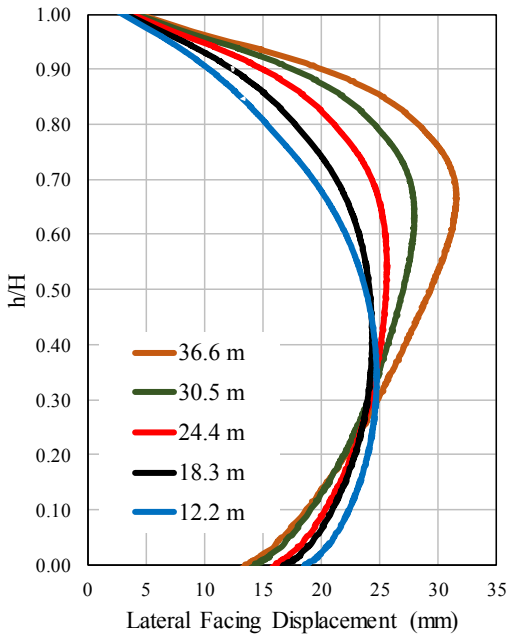

Fig. 4. Effect of span length on the lateral facing displacement.

4 Effect of reinforcement spacing

Four different reinforcement spacings, S_v, were considered and evaluated in this study: 0.1 m, 0.2 m, 0.3 m, and 0.4 m. Fig. 5 presents the strain distribution along the reinforcement at 20 and 80% of the abutment height as measured from the bottom of the abutment. It can be seen that for all cases the maximum strain envelope is located very close to the abutment face at 0.2 *H* of the abutment height and moves to about 1.2 m away from the abutment face at 0.8 *H*. However, the magnitude of maximum strain increases with increasing the reinforcement spacing. The maximum strain increases from 0.62% for a reinforcement spacing of 0.1 m to 1.63% for a reinforcement spacing of 0.4 m at 0.8 *H* from bottom of abutment. Fig. 6 presents the effect of the reinforcement spacing on the lateral facing displacement. The maximum lateral facing displacement increases from 28 mm for a reinforcement spacing of 0.2 m to about 42 mm for a reinforcement spacing of 0.4 m. The figures indicate that the reinforcement spacing has a significant influence on the strain distribution along the reinforcement and the lateral facing displacement for the same span length (36.6 m) and same abutment height (7.0 m) under the service loading condition.

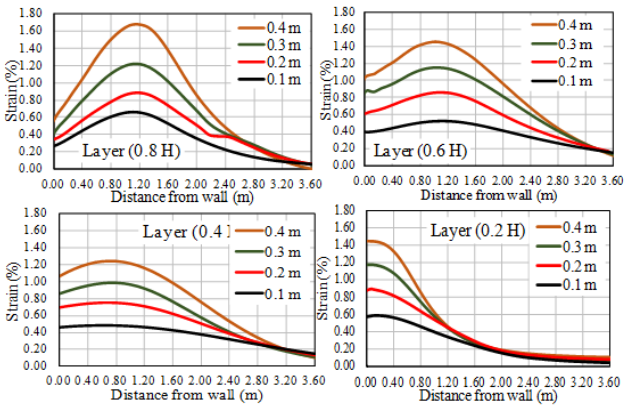

Fig. 5. Effect of reinforcement spacing on the strain distribution along geosynthetics.

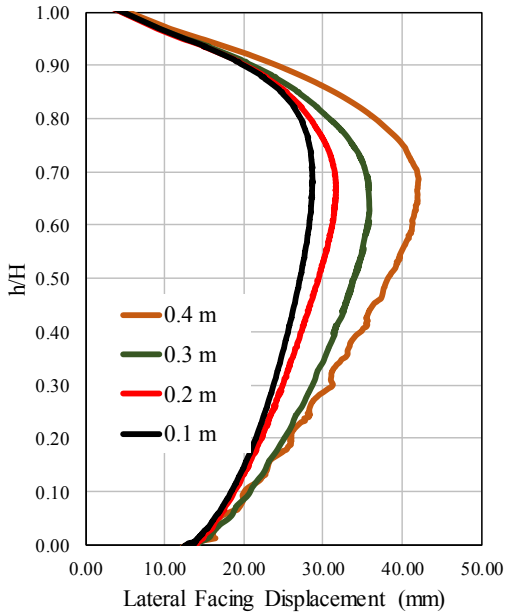

Fig. 6. Effect of reinforcement spacing on the lateral facing displacement.

5 Effect of reinforcement stiffness

Five different reinforcement stiffness, *EA*, were considered and evaluated in this study: 300, 600, 900, 1200, and 1500 kN/m. Fig. 7 presents the strain distribution along the reinforcement at 20, 40, 60, and 80% of the abutment height as measured from the bottom of abutment. Similar to the effect of reinforcement spacing, the reinforcement stiffness affects the magnitude of the strain but does not affect either the shape of the strain distribution or the location of maximum strain. The maximum strain decreases from about 1.3% for a reinforcement stiffness of 300 kN/m to about 0.5% for a reinforcement stiffness of 1500 kN/m. It can be seen that increasing the reinforcement stiffness from 300 kN/m to 900 kN/m has significant effect on the reinforcement strain (e.g., the strain decreases from 1.3% to 0.68% at 0.8 *H*). However, after that, the effect of reinforcement stiffness tends to decrease (e.g., the strain decreases from 0.6% to 0.5% when the reinforcement stiffness increases from 900 kN/m to 1500 kN/m at 0.8 *H*). Fig. 8 presents the effect of reinforcement stiffness on the lateral displacement of wall facing. The maximum lateral facing displacement decreases from 37 mm for a reinforcement stiffness of 300 kN/m to 26 mm for a reinforcement stiffness of 1500 kN/m.

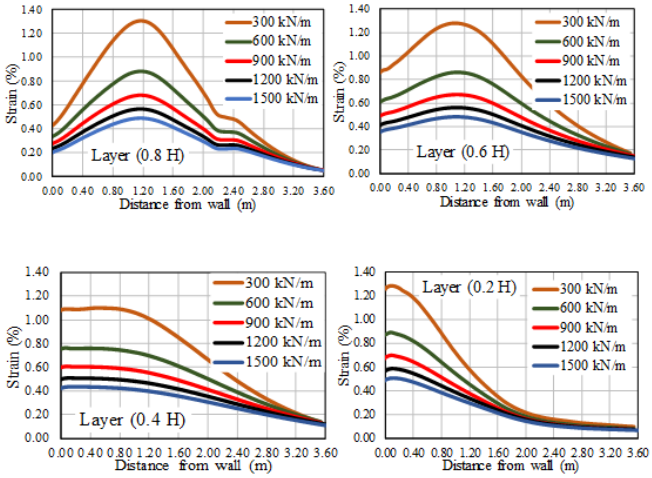

Fig. 7. Effect of reinforcement stiffness on the strain distribution along geosynthetics.

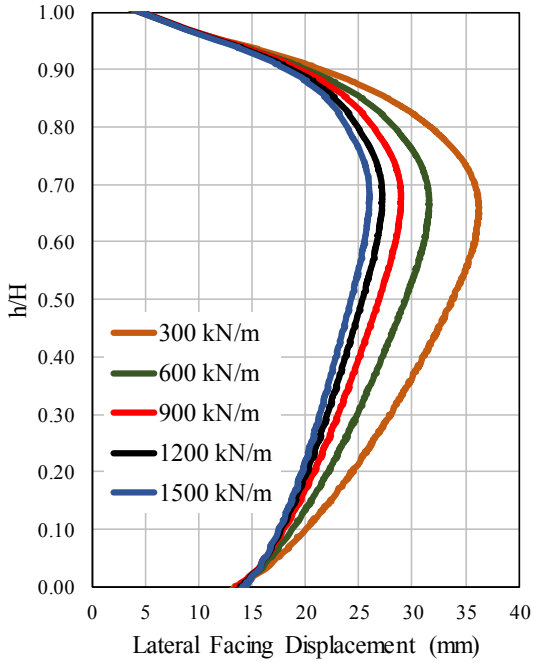

Fig. 8. Effect of reinforcement stiffness on the lateral facing displacement.

6 Conclusions

Finite element parametric study was conducted to evaluate the performance of the GRS-IBS in terms of lateral deformation and reinforcement strain. The parameters included in this study are the effects of span length, the height of GRS abutment, the reinforcement spacing, and the reinforcement stiffness. Based on the finding of this study, the following conclusions can be made:

- The magnitude of maximum strain is directly related to the location of the reinforcement within the same model, in which the reinforcement layers at the bottom have higher strains than those in the top layers. For example, the maximum strain decreases from 1.4% at 20% of the abutment height to 0.7% at 80% of the abutment height for the 7-m abutment height.
- The bridge span length has a significant effect on the GRS-IBS performance such that the magnitude of maximum strain and lateral facing displacement increase with increasing the span length. The maximum strain increases from 0.4% for span length of 12.2 m to about 0.9% for a span length of 36.6 m at 0.6 *H* above the bottom of the abutment, and the lateral facing displacement increases from 12 mm for a 12.1 m span length to 30 mm for a 36.6 m span length. The results indicate that while the magnitude of reinforcement strain is affected by span length and abutment height, the shape of the strain distribution is not affected.
- The reinforcement spacing has significant influence on the strain distribution along the reinforcement and the lateral facing displacement, in which the maximum strain and lateral facing displacement increase with increasing reinforcement spacing. The maximum strain increases from 0.6% for a reinforcement spacing of 0.1 m to 1.4% for a reinforcement spacing of 0.4 m, and the maximum lateral facing displacement increases from 28 mm for a reinforcement spacing of 0.2 m to 42 mm for a reinforcement spacing of 0.4 m.
- The reinforcement stiffness has significant influence on the behavior of GRS-IBS in terms of reducing the lateral facing displacement and the magnitude of strain distribution along the reinforcement with increasing stiffness up to a certain point, after which this impact tends to decrease in contrary to the effect of reinforcement spacing, which shows a constant impact on the performance of GRS-IBS.

This research project was funded by the Louisiana Transportation Research Center (LTRC Project No. 13-5GT) and Louisiana Department of Transportation and Development, LA DOTD (State Project No. 30000981). The authors would like to express their thanks to Zhongjie Zhang at LTRC for providing valuable help and support in this study.

References

1. Schanz, T., Vermeer, P.A., and Bonnier, P.G., (1999). The hardening soil model: formulation and verification. Beyond 2000 in computational geotechnics, 281-296.
2. Abu-Hejleh, N., Wang, T., and Zornberg, J.G., (2000). Performance of geosynthetic-reinforced walls supporting bridge and approaching roadway structures. In: Advances in transportation and geoenvironmental systems using geosynthetics, 218-243.
3. Adams, M., (1997). Performance of a prestrained geosynthetic reinforced soil bridge pier. Mech. Stab. backfill, 35-53.
4. Ketchart, K., (1997). Performance of geosynthetic-reinforced soil bridge pier and abutment, Denver, Colorado, USA. Mechanically stabilized backfill, 101-116.
5. Adams, M.T., Lillis, C.P., Wu, J.T.H., and Ketchart, K., (2002). Vegas mini pier experiment and postulate of zero volume change. In: Proceedings, Seventh International Conference on Geosynthetics, 389-394.
6. Adams, M.T., Ketchart, K., and Wu, J.T., (2007). Mini pier experiments: Geosynthetic reinforcement spacing and strength as related to performance. In: Geosynthetics in Reinforcement and Hydraulic Applications, 1-9.
7. Saghebfar, M., Abu-Farsakh, M., Ardah, A., Chen, Q., and Fernandez, B.A., (2017a). Performance monitoring of Geosynthetic Reinforced Soil Integrated Bridge System (GRS-IBS) in Louisiana. Geotextiles and Geomembranes, **45**(2), 34-47.
8. Saghebfar, M., Abu-Farsakh, M.Y., Ardah, A., Chen, Q., and Fernandez, B.A., (2017b). Full-Scale Testing of Geosynthetic-Reinforced, Soil-Integrated Bridge System. Transportation Research Record: Journal of the Transportation Research Board, (2656), 40-52.
9. Abu-Farsakh, M., Saghebfar, M., Ardah, A., and Chen, Q., (2017). A Case Study on Evaluating the Performance of a Geosynthetic Reinforced Soil Integrated Bridge System (GRS-IBS). In: Geotechnical Frontiers, 12-22.
10. Abu-Farsakh, M., Ardah, A., and Voyiadjis, G., (2018a). 3D Finite element analysis of the geosynthetic reinforced soil-integrated bridge system (GRS-IBS) under different loading conditions. Transportation Geotechnics, **15**, 70-83.
11. Abu-Farsakh, M., Ardah, A., and Voyiadjis, G., (2018b). Numerical Investigation of the Performance of Geosynthetic Reinforced Soil–Integrated Bridge System (GRS-IBS) Subjected to Differential Settlement (No. 18-01788).
12. Ardah, A., Abu-Farsakh, M., and Voyiadjis, G., (2017). Numerical evaluation of the performance of a Geosynthetic Reinforced Soil-Integrated Bridge System (GRS-IBS) under different loading conditions. In: Geotextiles and Geomembranes.
13. Ardah, A., Abu-Farsakh, M.Y., and Voyiadjis, G.Z., (2018). Numerical Evaluation of the Effect of Differential Settlement on the Performance of GRS-IBS. Geosynthetics International, 1-45.
14. Adams, M., Nicks, J., Stabile, T., Wu, J., Schlatter, W., and Hartmann, J., (2011). Geosynthetic Reinforced Soil Integrated Bridge System, Interim Implementation Guide (No. FHWA-HRT-11-026).
15. Ling, P., and Leshchinsky, D., (1996). Mesa Walls: Field Data Reduction, Finite Element Analysis, and Preliminary Design Recommendations. Report to Tensar Earth Technologies, Inc., Atlanta, GA, February 1.

16. Leshchinsky, D., and Vulova, C., (2001). Numerical investigation of the effects of geosynthetic spacing on failure mechanisms in MSE block walls. Geosynthetics International, **8**(4), 343-365.
17. Holtz, R.D., and Lee, W.F., (2002). Internal stability analyses of geosynthetic reinforced retaining walls (No. WA-RD 532.1,). Olympia, Washington: Washington State Department of Transportation.
18. Guler, E., Hamderi, M., and Demirkan, M.M., (2007). Numerical analysis of reinforced soil-retaining wall structures with cohesive and granular backfills. Geosynthetics International, **14**(6), 330-345.
19. Huang, J., Han, J., Parsons, R.L., and Pierson, M.C., (2013). Refined numerical modeling of a laterally-loaded drilled shaft in an MSE wall. Geotextiles and Geomembranes, **37**, 61-73.
20. Mirmoradi, S.H., and Ehrlich, M., (2014a). Modeling of the compaction-induced stresses in numerical analyses of GRS walls. International Journal of Computational Methods, **11**(02): 1342002.
21. Mellas, M., Mabrouki, A., Benmeddour, D., and Rahmouni, O., (2015). Numerical study of geogrid-reinforced segmental earth retaining wall. Journal of Applied Engineering Science & Technology, **1**(2), 43-49.
22. Rahmouni, O., Mabrouki, A., Benmeddour, D., and Mellas, M., (2016). A numerical investigation into the behavior of geosynthetic-reinforced soil segmental retaining walls. International Journal of Geotechnical Engineering, **10**(5), 435-444.
23. Wu, J.T., Lee, K.Z., and Pham, T., (2006). Allowable bearing pressures of bridge sills on GRS abutments with flexible facing. Journal of Geotechnical and Geoenvironmental Engineering, **132**(7), 830-841.
24. Wu, J.T., Yang, K.H., Mohamed, S., Pham, T., and Chen, R.H., (2014). Suppression of soil dilation—A reinforcing mechanism of soil-geosynthetic composites. Transportation Infrastructure Geotechnology, **1**(1), 68-82.
25. Liu, H., (2015). Reinforcement load and compression of reinforced soil mass under surcharge loading. Journal of Geotechnical and Geoenvironmental Engineering, **141**(6), p.04015017.
26. Zheng, Y. and Fox, P.J., (2016). Numerical Investigation of Geosynthetic-Reinforced Soil Bridge Abutments under Static Loading. Journal of Geotechnical and Geoenvironmental Engineering, **142**(5), p.04016004.
27. Zheng, Y. and Fox, P.J., (2017). Numerical Investigation of the Geosynthetic Reinforced Soil–Integrated Bridge System under Static Loading. Journal of Geotechnical and Geoenvironmental Engineering, **143**(6), p.04017008.
28. Brinkgreve, R.B.J. (Ed.). (2002). Plaxis: Finite Element Code for Soil and Rock Analyses: 2D-Version 8: [user's Guide]. Balkema.
29. Dantas, B.T. (2004). Working Stress Analysis Method for Reinforced Cohesive Soil Slopes (Doctoral dissertation, D. Sc. Thesis, COPPE/UFRJ, Rio de Janeiro (in portuguese)).
30. Ehrlich, M., and Mirmoradi, S.H. (2013). Evaluation of the effects of facing stiffness and toe resistance on the behavior of GRS walls. Geotextiles and Geomembranes, **40**: 28-36.
31. Mirmoradi, S. H., and Ehrlich, M. (2014b). Numerical evaluation of the behavior of GRS walls with segmental block facing under working stress conditions. Journal of Geotechnical and Geoenvironmental Engineering, **141**(3): 04014109.
32. Ardah, A., (2018). Field Instrumentations and Numerical Analysis of Geosynthetic Reinforced Soil – Integrated Bridge System (Grs-Ibs).
33. Ling, H.I., Yang, S., Leshchinsky, D., Liu, H., and Burke, C., (2010). Finite-element simulations of full-scale modular-block reinforced soil retaining walls under earthquake loading. Journal of engineering mechanics, **136**(5), 653-661.
34. Abu-Farsakh, M., Ardah, A., and Voyiadjis, G., (2018) Numerical Investigation of the Performance of a Geosynthetic Reinforced Soil-Integrated Bridge System (GRS-IBS) under Working Stress Conditions. In IFCEE 2018, 76-87.